PAPER

Reduced energetic particle transport models enable comprehensive time-dependent tokamak simulations

IOP Publishing | International Atomic Energy Agency Nuclear Fusion

Nucl. Fusion **59** (2019) 106013 (13pp) https://doi.org/10.1088/1741-4326/ab3112

Reduced energetic particle transport models enable comprehensive time-dependent tokamak simulations

M. Podestà[1], L. Bardóczi[2,3], C.S. Collins[2], N.N. Gorelenkov[1], W.W. Heidbrink[4], V.N. Duarte[1], G.J. Kramer[1], E.D. Fredrickson[1], M. Gorelenkova[1], D. Kim[1], D. Liu[4], F.M. Poli[1], M.A. Van Zeeland[2] and R.B. White[1]

[1] Princeton Plasma Physics Laboratory, Princeton NJ 08543, United States of America
[2] General Atomics, PO Box 85608, San Diego, CA 92186, United States of America
[3] Oak Ridge Associated Universities, Oak Ridge, TN 37831, United States of America
[4] Department of Physics and Astronomy, University of California Irvine, Irvine, CA 92697, United States of America

E-mail: mpodesta@pppl.gov

Received 28 January 2019, revised 13 May 2019
Accepted for publication 9 July 2019
Published 21 August 2019

Abstract

Time-dependent integrated simulations through codes such as TRANSP are becoming an indispensable tool for the interpretation of existing experiments and predictions of optimized scenarios. For many practical cases, quantitative simulations need to include the effect of plasma instabilities on the evolution of a tokamak discharge. An example is the degradation in energetic particle (EP) confinement induced by instabilities, which in turn affects important source terms for heating, non-inductive current, and momentum in a simulation. The reduced-physics *kick model* provides phase-space resolved transport probability matrices to TRANSP that are used to account for enhanced EP transport by instabilities in addition to neoclassical transport. The model has recovered the measured Alfvén eigenmode (AE) spectrum on NSTX, NSTX-U and DIII-D, and has reproduced details of phase-space resolved fast ion diagnostic data measured on DIII-D for EP-driven modes and tearing modes. In general, the kick model has proven the potential of phase-space resolved EP simulations to unravel details of EP transport for detailed theory/experiment comparison and for scenario planning based on optimization of neutral beam injection parameters. In this work, the extension of the kick model to low-frequency instabilities such as tearing modes and fishbones, in addition to AEs, is assessed. The goal is to enable TRANSP simulations that retain the main effects of multiple types of instabilities through a common framework. Results from the NSTX/NSTX-U and DIII-D tokamaks show that the extension to *multi-mode* scenarios can expand the range of applicability of the model for more reliable, quantitative integrated simulations.

Keywords: energetic particle transport, Alfvén instabilities, integrated tokamak simulations, low-frequency MHD

(Some figures may appear in colour only in the online journal)

1. Introduction

Validated quantitative predictions of tokamak scenarios are required to explore the operational space of fusion reactors such as ITER and DEMO [1]. As plasma performance improves towards *burning* plasmas, the importance of predicting the behavior of highly energetic particles (EPs)—e.g. from fusion reactions, neutral beam injection (NBI) and rf waves—increases. In fact, energetic particles are expected to be the dominant source of heating and momentum for burning plasmas. Although NBI and rf waves are reliable tools for heating and current drive, the resulting EP population can destabilize Alfvénic (AEs) and other magneto-hydrodynamic (MHD) instabilities [2–6]. The latter typically cause a degradation in performance and, if significant EP losses are induced, can lead to damage of vacuum vessel components.

As an example, results from a NSTX-U [7] discharge featuring several EP-driven instabilities are shown in figure 1, which is further discussed in section 3.3. Considerable degradation of plasma performance can be inferred from the reduction in neutron rate, fast ion density and NB driven current with respect to *classical* simulations that do not include the enhanced EP transport by instabilities. Notably, however, different EP transport models can provide substantially different results e.g. in terms of radial profiles of EP density (figure 1(*d*)), even if modeled global quantities such as the neutron rate are nearly indistinguishable. This motivates the adoption of physics based—as opposed to *ad-hoc*—models, that need to be subject to strict benchmark against first-principles simulations and validation against experiments.

At present, numerical codes can predict the spectrum of Alfvénic instabilities (AEs) that is expected for a given scenario [4, 5, 8] and the EP transport that results from a given AE spectrum. A remaining challenge is to develop quantitative methods to compute AE stability, saturation amplitude and associated EP transport in time-dependent transport codes that are able to predict a whole plasma discharge. *Reduced* models are an effective tool to distill information from theory and first-principles codes and implement numerically efficient methods to investigate AE stability and fast ion transport [9–14]. With respect to first-principles codes, reduced models are less computationally intensive while still retaining the relevant physics for the effects of instabilities on EP evolution, thus enabling long-time-scale simulations at reduced computational cost. Two approaches are currently being pursued at PPPL for the development of predictive, reduced EP transport models for integrated simulation codes such as TRANSP [15–18]. A first approach relies on numerical tools to distill information on EP transport that can then be used in TRANSP. This is the basis for the *kick model* [13, 19]. A second approach is based on the quasi-linear theory for wave-particle interaction [20] extended to include the resonance frequency broadening as the mode amplitude increases [9, 21] and the effects of multiple resonances. This approach has resulted in the development of the RBQ-1D model [14, 22]. Being based on a numerical approach not constrained by the quasi-linear approximation, the kick model enables a more general approach to fast ion transport than RBQ-1D. However, this also results in more computationally expensive simulations. By comparing results from the two models and their respective limits of validity, future directions for a computationally efficient transport model can be more easily identified.

Initial studies with kick and RBQ-1D models have highlighted the importance of including EP phase space effects to analyze and interpret the stability properties of Alfvénic modes and associated transport. For example, the competition between gradients in the EP distribution along both energy and canonical angular momentum cannot be captured by simpler models solely based on AE drive by radial gradients of the EP population (so-called *critical gradient models* [10, 11]) or gradients in the velocity variable only [23, 24]. The latter effects are especially important in plasmas with NB injection—such as those of NSTX-U, DIII-D [25] and most present-day tokamaks—due to the strongly non-isotropic EP distribution. Phase space resolution is also crucial for a quantitative validation of the models against fast ion diagnostics, e.g. fast ion D-Alpha (FIDA) and neutral particle analyzers (NPA).

This work focuses on results from the kick model, and in particular on its extension to include the effects of low-frequency instabilities in addition to Alfvénic modes. Recent work has shown the potential of the model to capture EP transport by neoclassical tearing modes (NTMs) [26, 27] and sawteeth [28]. The goals here are to provide a comprehensive assessment of the capabilities of the model to include the effects of NTMs on fast ion transport, extend the model to fishbones, and test the resulting TRANSP + kick model analysis in a scenario that features more than one type of instabilities, for example AEs and fishbones. In this regard, using the same model to treat all instabilities based on a common framework is expected to improve the reliability of the simulations.

In the remainder of this work, recent advances in the modeling tools are first introduced in section 2. Section 3 presents examples of the application of those tools to interpret discharges from NSTX-U and DIII-D, including their extension to include effect of instabilities other than Alfvénic modes. A brief discussion on the application of the models for *predictive* analysis is given in section 4. The main results of this work are summarized in section 5.

2. Modeling tools for interpretive EP transport analysis

Fast ion modeling in TRANSP is performed through the Monte Carlo module NUBEAM [17, 18], which includes classical phenomena such as collisional scattering and slowing-down, and atomic physics (e.g. charge-exchange and neutralization reactions). In recent years, NUBEAM has been updated to include two physics-based reduced models to account for resonant EP transport by instabilities, namely the *kick* [13, 19] and *RBQ-1D* [14, 22] models. Both models share the same input files for NUBEAM and the same prescription for EP transport coefficients through transport probability matrices, see section 2.1.

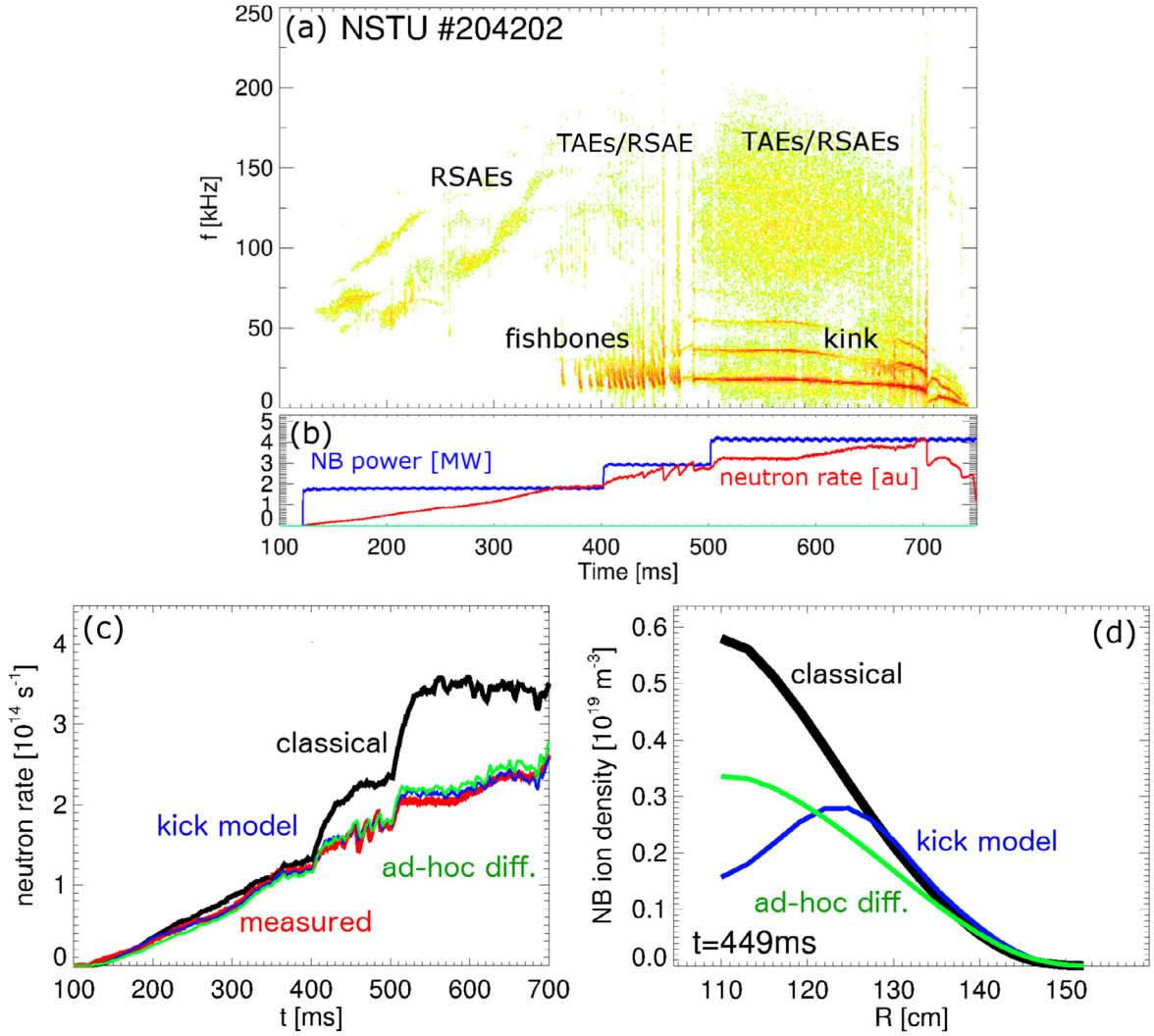

Figure 1. (*a*) Magnetic fluctuations spectrum from NSTX-U discharge #204202. Several types of EP-driven instabilities are observed. (*b*) Waveform of injected NB power and measured neutron rate. (*c*) TRANSP results for classical simulations (black) and simulations including the effects of instabilities on EP transport through the physics-based *kick model* (blue) and a simple *ad-hoc* diffusive model (green). The measured neutron rate is shown in red. (*d*) Profiles of fast ion density around $t = 450$ ms.

The primary input for NUBEAM is a set of transport probability matrices that condense the effects of instabilities on EP dynamic. Matrices are defined over the phase-space constant of motion variables E, P_ζ and μ, which represent the EP energy, canonical toroidal angular momentum and magnetic moment [29, 30]. For each (E, P_ζ, μ) region, the matrix contains a probability $p(\Delta E, \Delta P_\zeta)$ of correlated fast ion energy and P_ζ changes (or *kicks*) caused by the instabilities. Each probability matrix can represent a single perturbation or a set of perturbations with similar temporal evolution.

For the kick model, the transport matrix is computed via particle following codes such as the Hamiltonian guiding-center code ORBIT [31]. For Alfvénic modes that can feature a large number of poloidal harmonics and a complex radial mode structure, mode structures are computed through MHD codes such as NOVA/NOVA-K [32–34]. Low-frequency modes such as NTMs and fishbones are usually characterized by simpler mode structures that can be approximated by analytical expressions. To compute a kick probability matrix in ORBIT, the EP phase space is divided into discrete bins to group particles with similar phase space coordinates. Typical numbers of bins for the E, P_ζ and μ are $n_E \sim 10$–15, $n_{P_\zeta} \sim 30$–40 and $n_\mu \sim 14$–20 respectively. The evolution of (E, P_ζ, μ) of each particle is recorded in ORBIT during the simulation at sampling intervals $\delta t_{\rm samp}$. The value of $\delta t_{\rm samp}$ is chosen to be larger than the period of the instability to filter out fast oscillations and mostly retain changes over the longer time scales associated with particles being trapped in a resonance. Eventually, thousands of $\Delta E, \Delta P_\zeta$ samples are accumulated for each phase space bin. These samples are used to compute the two-dimensional histogram $p(\Delta E, \Delta P_\zeta)$ on a finite ΔE, ΔP_ζ grid Once the procedure is extended to the whole phase space, the result is a five-dimensional transport matrix $p(\Delta E, \Delta P_\zeta | E, P_\zeta, \mu)$. More details on the kick model simulations in ORBIT are given in the appendix of [13].

To compute the probability, the mode amplitude is kept constant during the ORBIT simulation at a level that corresponds to typical measured amplitudes. This amplitude level

is taken as the reference $A_{\rm mode} = 1$ for the TRANSP + kick model analysis.

2.1. Implementation of the kick model in TRANSP

The kick model has been expressly developed to fit within the Monte Carlo implementation of NUBEAM. As discussed in the previous section, wave-particle interaction processes are distilled through modeling with the particle-following code ORBIT into *kick probability matrices*, $p(\Delta E, \Delta P_\zeta | E, P_\zeta, \mu)$. Information on magnetic equilibrium, plasma profiles and heating sources is passed from TRANSP to NUBEAM at the beginning of a NUBEAM time step k. Inputs from the kick model (probability matrices and amplitude evolution) are also loaded. From step k to step $k+1$, a representative ensemble of fast ions is evolved. The particle ensemble is updated based (primarily) on active NB sources and sinks, such as losses, re-neutralization and thermalization. In addition, particle variables are mapped in phase space to compute the kick model corrections to the particle's orbit. Knowing its (E, P_ζ, μ) variables, kicks ΔE and ΔP_ζ are sampled randomly from each transport probability matrix. The E and P_ζ kicks are rescaled based on the amplitude scaling factor input to mimic time-varying amplitude of the modes.

Several kicks are applied during the particle's orbiting in NUBEAM, along with effects of collisional processes. Typically, between tens to hundreds of kicks are applied to particles with a finite kick probability during a NUBEAM macroscopic time step of 1–5 ms. After each kick, the remaining particle's variables are updated to reflect changes in energy and canonical toroidal momentum. For instance, the radial position, pitch and kinetic energy are updated. (The magnetic moment is assumed to be conserved given that the frequency of the instabilities considered here is well below the ion cyclotron frequency). At present, the mode amplitude scaling factors $A_{\rm mode}(t)$ are given as input to TRANSP/NUBEAM and are not self-consistently updated during a simulation based on the power exchanged between the sample EP population and the modes. However, that information is recorded and made available as TRANSP output, which makes it possible to infer useful information on mode drive and overall stability (see example in section 3.3).

The evolution of the fast ion ensemble under classical physics and kick model effects is repeated until the end of step k, at which time quantities such as fast ion density, power from thermalization, NB-driven current are computed. TRANSP parameters are then updated, for instance by recomputing the magnetic equilibrium based on total current evolution, and made available for the next NUBEAM step.

2.2. Extension of the kick model to NTMs and fishbones

The kick model was initially developed to account for enhanced EP transport by Alfvénic instabilities such as TAEs and RSAEs [13, 19]. A similar approach has been recently extended to include the effects of low-frequency instabilities such as kink modes, fishbones, sawteeth [28] and NTM [27].

Although validation work is ongoing to assess the limitations of the approach and possible improvements to the model, initial results are encouraging, see [27, 28]. This section summarizes the main aspects of the extension of the kick model to low-frequency instabilities. Initial TRANSP simulations including kick model treatment of NTMs and fishbones are then discussed in section 3, which concludes with the analysis of a multi-mode NSTX-U discharge with simultaneous fishbones and AEs.

Compared to Alfvénic modes, low-frequency instabilities present specific features that justify a thorough re-examination and validation of the transport models previously used for TAE/RSAE modes only. Information on the radial structure of perturbations is specified in ORBIT by supplying a set of $\alpha_{n,m}(\Psi)$ or $\xi_{n,m}(\Psi)$ coefficients for each (n,m) pair of toroidal/poloidal mode numbers. The α's are related to the radial structure of the magnetic field perturbation through $\delta\mathbf{B} = \nabla \times \alpha\mathbf{B}$, with $\alpha(\Psi, t) = \Sigma_{n,m}\alpha_{n,m}(\Psi)sin(n\zeta - m\theta - \omega t)$ (ζ: toroidal angle, θ: poloidal angle, ω: angular mode frequency) [35]. Similarly, the radial displacement $\xi_{n,m}(\Psi)$ can be used, with $\delta\mathbf{B} = \nabla \times (\xi \times \mathbf{B})$. For NTMs, the $\alpha_{n,m}$ coefficients are approximated with a simple gaussian peaked at the rational surface $q = m/n$, with (m,n) deduced from the experiment [36]. (A more sophisticated model for the α's and a comparison with the simple approach adopted herein are discussed in [27]). For fishbones, a hat-like radial displacement $\xi_{1,1}(\Psi)$ is used, see discussion of figure 2 below.

The $\alpha(\Psi, t)$ and $\xi(\Psi, t)$ representations have been widely used in ORBIT to describe ideal MHD modes and their effects on EP transport. A direct implication of representing modes within ideal MHD is that the electric field parallel to $\mathbf{B}$ must be zero. For time varying α's, this condition is enforced in ORBIT by balancing the field induced by the perturbation through a potential of opposite sign [29]. For perturbations such as NTMs, resistive effects are expected in a thin layer around rational surfaces [37]. Those effects are neglected in the present treatment of NTMs within the kick model.

For fishbones, three different EP transport models are tested in the following. The main difference among models is how different regions of fast ion phase space are affected by the fishbones. In the fishbone model originally introduced in TRANSP[5], the fraction of fast particles redistributed by the mode can be set as input. Under the assumption that the main (bounce) resonance driving the mode involves trapped fast ions, only deeply trapped particles are affected for increasingly small fractions. For example, a fraction of 25% gives a reasonable agreement in terms of measured versus simulated neutron rate for the NSTX scenarios analyzed so far, see example in section 3.2. A second model uses a radially uniform, possibly time varying diffusivity to enhanced fast ion transport. In its simplest implementation adopted here, the model acts on all fast ions independently of their phase space localization. For NSTX, diffusivities $D_b = 0.5$–2 m^2 s^{-1} are typically required to match the measured neutron rate. In the kick model, fishbones are modeled with an analytical hat-like

[5] For more details please refer to the TRANSP help following the link from https://transp.pppl.gov.

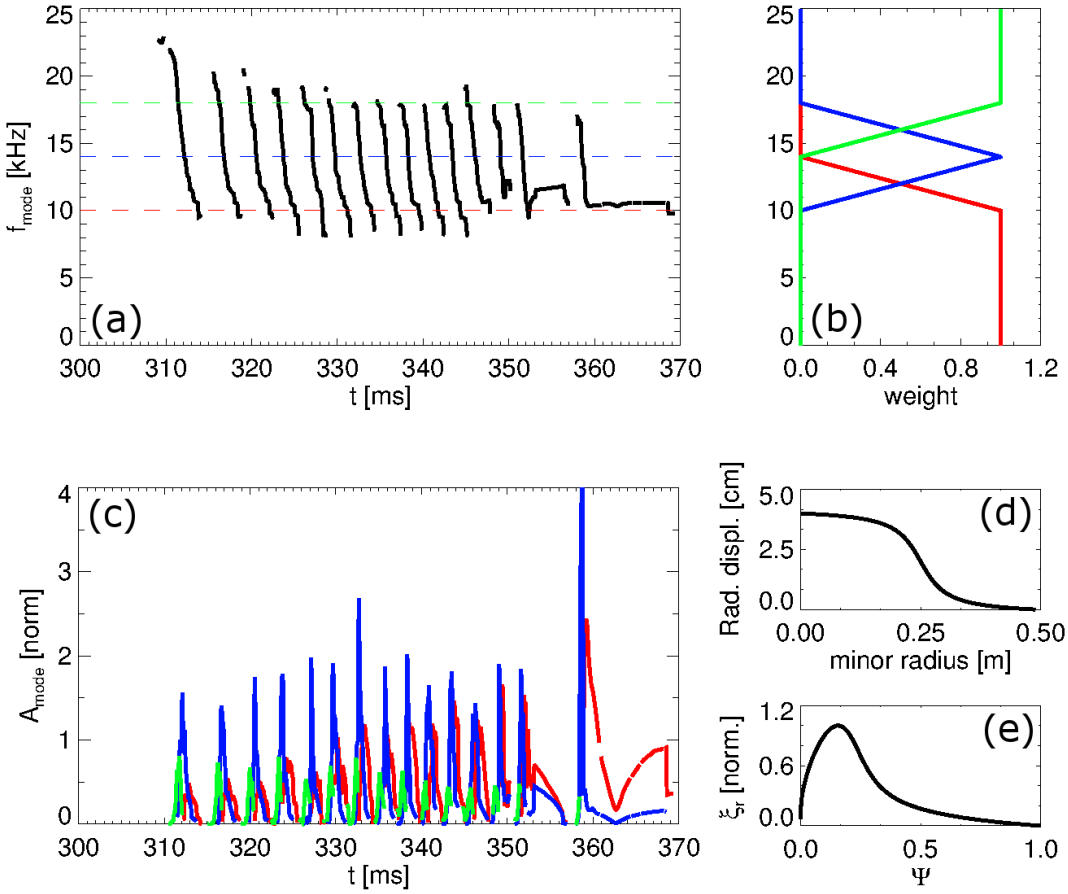

Figure 2. Schematic of the procedure used to represent frequency-sweeping fishbones as a set of three sub-modes, each with constant frequency, to be used in the kick model. (*a*) Mode frequency versus time extracted from Mirnov coils data. (*b*) Weight factors for each sub-mode as a function of frequency. (*c*) The total mode amplitude from Mirnov coils data is weighted by each of the three weight factors, with their sum representing the original mode. (*d*) Radial displacement versus minor radius with $r_0 = 0.25$ m and $\Delta r_0 = 0.04$ m, and (*e*) corresponding normalized displacement mapped on the poloidal flux variable as used in ORBIT simulations.

radial structure assuming dominant toroidal and poloidal mode numbers $n = 1$ and $m = 1$ for the instability.

The rapid variations in both amplitude and frequency of fishbones, occurring over time scales of milliseconds, challenge the phase-space representation from kick model in two ways. First, mode frequency variations would alter the location of resonance(s) in phase space, whereas the kick model typically computes resonances for fixed-frequency modes; second, large amplitude excursions imply that the radial extent of resonances vary dynamically, whereas kick model inputs are usually computed for fixed mode amplitudes near the experimental values. To address those features, each fishbone cycle is decomposed as the superposition of $N_{\rm sub}$ sub-modes each characterized by a fixed frequency f_i, $i = 1...N_{\rm sub}$ as shown in figure 2. Given the measured mode frequency and amplitude (from Mirnov coils), $f(t)$ and $A(t)$, a linear weight $w_i(t)$ is defined for the ith sub-mode at frequency f_i:

$$w_i(t) = \begin{cases} 1 - \frac{|f - f_i|}{\Delta f}, f_{i-1} \leqslant f \leqslant f_{i+1} \\ 0, f < f_{i-1} \; or \; f > f_{i+1} \end{cases} \qquad (1)$$

where $\Delta f = |f_i - f_{i-1}|$. To cover the entire frequency range, the weight for the highest-frequency sub-mode is set to $w_i \equiv 1$ for frequencies larger than the maximum f_i (and similarly for the lowest-frequency sub-mode), see figure 2(*b*). Individual amplitudes to be used in the kick model are then computed as $A_i = w_i(t)\,A(t)$, with typically $N_{\rm sub}$ =3–5 sub-modes.

The displacement induced by fishbones in terms of actual radius is approximated with an arc tangent expression centered at r_0 and with width Δr_0, see figure 2(*d*). The two parameters r_0, Δr_0 are estimated from experimental data, e.g. on NSTX/NSTX-U from soft x-ray measurements or from a reflectometer array. Knowing the equilibrium, the displacement is finally re-mapped in terms of the poloidal flux variable used in ORBIT simulations (figure 2(*e*)).

3. Analysis of fast ion transport in NSTX/NSTX-U and DIII-D plasmas

The following sections discuss examples of the analysis of NSTX/NSTX-U and DIII-D plasmas, including the corresponding physics insight that can be achieved through the use of reduced EP transport models.

Starting from instabilities with frequencies comparable to the local plasma rotation frequency, NTMs, kink modes and sawteeth are well known to enhance EP transport. Examples from NSTX and DIII-D discharges with unstable fishbones

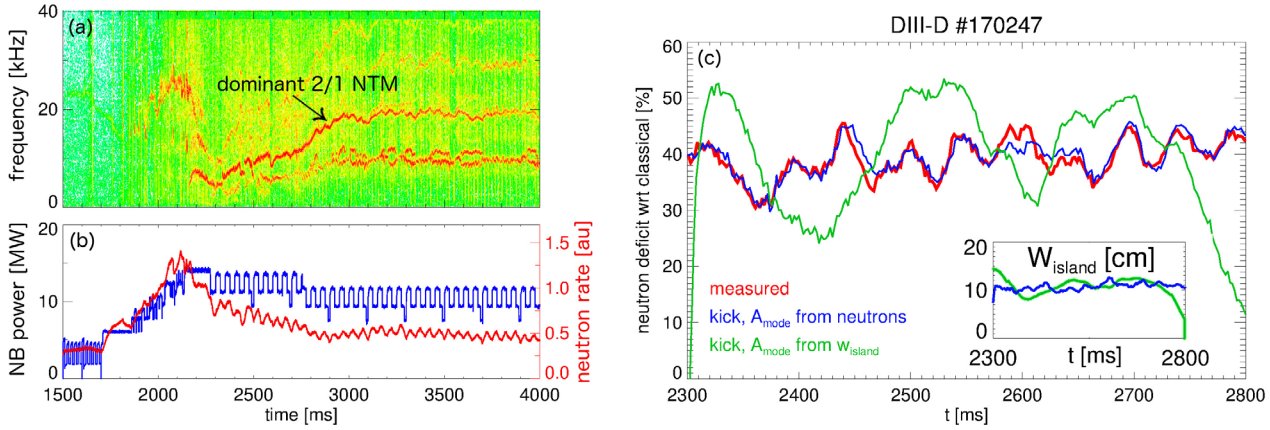

Figure 3. Analysis of DIII-D discharge #170247. (*a*) Magnetic fluctuation spectrum from Mirnov coils, showing the dominant $(m, n) = (2, 1)$ NTM instability. (*b*) Waveforms of injected NB power (blue) and measured neutron rate (red). (*c*) Deficit in the neutron rate from TRANSP modeling compared to the measured rate. The inset shows the mode amplitude, in terms of NTM island width, inferred from the interpretive kick model analysis matching the measured neutron rate (blue) and from a reconstruction of the NTM island width from ECE measurements (green).

and NTMs are discussed in sections 3.1 and 3.2. At higher frequency, Alfvénic instabilities (toroidal and reversed-shear AEs, TAEs and RSAEs) dominate the fluctuation spectrum. Based on previous work [13, 38–40] their effect on fast ion transport and results from the associated TRANSP + kick model analysis are briefly summarized at the end of section 3.2. Unlike the examples in sections 3.1 and 3.2, in many practical scenarios multiple types of instabilities can be simultaneously present. The example shown in figure 1 is further discussed in section 3.3 to illustrate the complexity of such multi-mode cases and how reduce models can address them.

3.1. Single-mode scenario: DIII-D plasmas with unstable NTMs

Figure 3 shows simulation results for a DIII-D discharge aimed at investigating fast ion transport by NTMs [26]. The discharge was specifically designed to trigger large amplitude $(m, n) = (2, 1)$ NTMs by stepping up the injected NB power, see figures 3(*a*) and (*b*). As the modes are destabilized, the measured neutron rate drops substantially. The deviation between measured and (classically) simulated neutron rate (figure 3(*c*) confirms the enhancement in fast ion transport and possibly in fast ion losses, with an average deficit in neutron rate of $\approx$40%.

Results from two simulations with the kick model are also shown in figure 3. For the first simulation, the NTM amplitude in the kick model is adjusted until a satisfactory agreement is achieved between simulated and measured neutron rate. In the second simulation, the NTM island width is inferred from experimental data from electron-cyclotron emission (ECE) and magnetic pickup coils [41, 42], then converted into the input mode amplitude for the kick model. The overall reduction in neutron rate is comparable for the two cases. In fact, the mode amplitude used for the interpretive simulation is within $\pm$10% from the amplitude directly inferred from the experiment, see inset in figure 3(*c*).

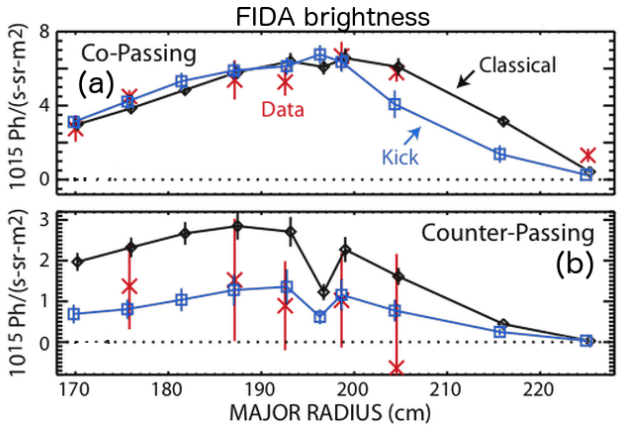

Figure 4. Radial profiles of FIDA brightness for (*a*) co-passing and (*b*) counter-passing fast ions from TRANSP (solid lines) and from experimental data (red symbols). Amplitudes in the kick model are rescaled to match the measured neutron rate. The magnetic axis is located at $R = 1.76$ m. The $q = 2$ surface, around which the 2/1 island is localized, is at $R \approx 2.1$ m. (Adapted courtesy of IAEA. Figure from [26]. Copyright (2018) IAEA).

Figures 4(*a*) and (*b*) show Fast-Ion D-Alpha measurements [43] compared to reconstructed signals based on the TRANSP output processed through the FIDAsim code [44]. The comparison reveals important features of fast ion transport in phase space. For co-passing fast ions, both experimental data and simulations indicate a weak effect of the instability. FIDA signals are close to those from the classical simulation for most of the radial positions for which data are available. Kick model results deviate from the classical case only for regions close to the $q = 2$ surface near $R = 2.1$ m where the mode is localized. Counter-passing fast ions, in turn, are strongly affected by the NTMs. The simulated reduction in FIDA signal of $\sim$50% is consistent with the measurements. Note that using a simple ad-hoc diffusivity would result in a similar depletion for co- and counter-passing fast ions, which would lead to a discrepancy between simulation and FIDA

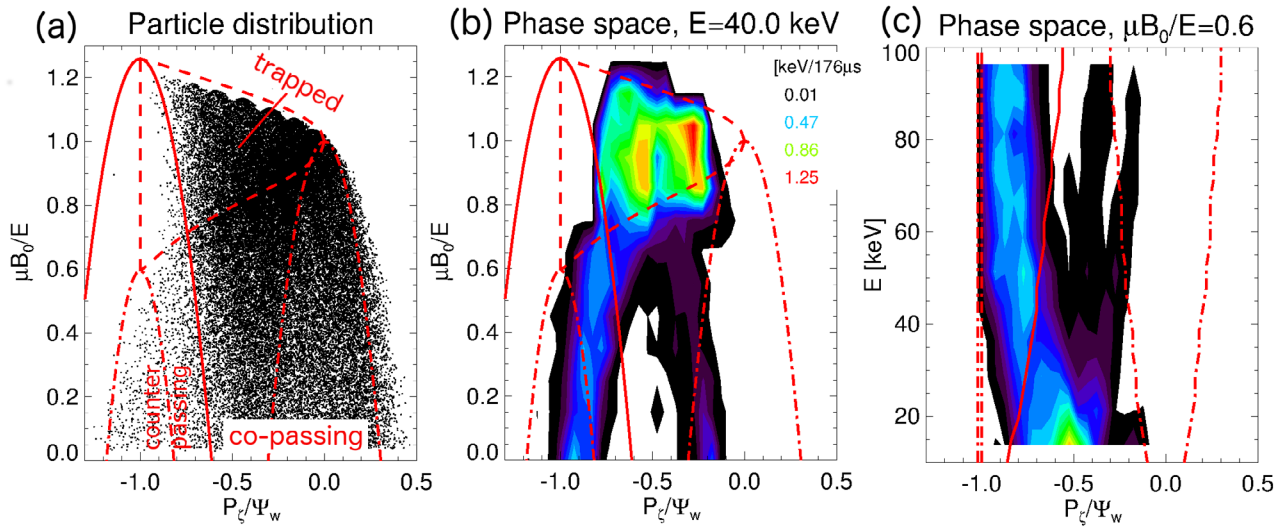

Figure 5. (*a*) Sample of the classical fast ion distribution for $E \geqslant 10$ keV during the NTM phase ($t \approx 2.5$ s) for DIII-D #170247. Phase space boundaries are computed for $E = 40$ keV. (*b*)–(*c*) Examples of average energy kicks versus phase space coordinates for the 2/1 NTM, as computed through ORBIT. Shown are two phase space cuts at (*b*) constant energy $E = 40$ keV and (*c*) constant $\mu B_0/E$ (normalized magnetic moment).

measurements. This confirms the requirement of phase-space resolved EP transport models to capture the correct fast ion response to instabilities.

The different response of co-passing versus counter-passing fast ions observed in the FIDA data can be qualitatively understood by considering the phase space dependence of NTM-induced transport, see figure 5. Only ≈1 MW of the average 10 MW power is injected in the counter direction. Therefore, NBI mostly populates the co-passing and trapped regions. The counter-passing region below the injection energy can be further populated as particles slow down and experience collisional scattering. However, for this scenario, the 2/1 NTM causes large transport for counter-passing particles at all energies, see figures 5(*b*) and (*c*), thus limiting the number of counter-passing particles over a broad region. Conversely, transport is limited for co-passing particles, which then experience more localized depletion around the peak mode location.

In addition to fast ion data at fixed times, time-dependent simulations offer the advantage of providing information on the dynamical response of fast ions and other related quantities to perturbations, either from instabilities or from external sources. Of particular value are experiments in which a known perturbation is applied, e.g. through modulation of the NB sources [45]. For the discharge in figure 3, a single NB source with on-axis tangential injection was modulated with a period of 50 ms and duty cycle 50%. Conditional sampling analysis of various signals and simulation outputs can thus be performed over a 1 s time window with nearly stationary conditions to infer correlations between mode behavior and fast ion response. The analysis can be used to further test the validity of the EP transport models in TRANSP, as well as to assess the effects of fast ions on the instabilities. The main results are shown in figure 6, which summarizes some of the findings originally discussed in [26]. The comparison between measured and simulated neutron rate (figure 6(*a*) confirms that TRANSP + kick model simulations do indeed achieve a very close match with the experimental neutron rate, which was the initial target for adjusting the mode amplitude input in the model.

The simulation predicts that the power transfer from EPs to the NTM increases by ≈20% as the NB power is increased by ≈24% (figure 6(*b*), suggesting that most of the newly injected NB ions interact with the mode. One could therefore assume that fast ions are directly destabilizing the NTM. In fact, results for the relative NTM amplitude variation during a NB modulation cycle indicate that the amplitude is increasing in both the experimental data and the simulation (figure 6(*c*). However, two observations lead to discard this simple conclusion. First, results for the mode amplitude variation show a large statistical uncertainty with no clear trend in the simulation results. Second, even if a clear trend seems to be present in the experimental data, the shape of the response to the modulation does not correlate with the shape of the power to the mode, which features a prompt increase at the NB turn-on. These observations suggest that the effect of fast ions on the NTM stability is—at best—weak and indirect. Results from the conditional analysis of background plasma quantities (as derived from the TRANSP input files) near the mode location support, at least in part, this conclusion, see figures 6(*d*)–(*f*). The same response of both plasma rotation and mode frequency to the NB modulation is observed, which is consistent with a simple increase in the Doppler shift of the mode frequency as measured in the lab frame. Local electron density and temperature increase, which may result in an increased neoclassical drive for the NTM. Changes are small, however: $\delta n_e/n_e \sim 1\%$ and $\delta T_e/T_e \sim 4.5\%$. A more detailed analysis of the NTM drive mechanisms, including a reconstruction of the evolution of pressure gradients to compute the NTM drive, is beyond the scope of this work. However, the previous example shows how time-dependent simulations with a physics-based model for EP transport can provide additional information to complement direct experimental measurements.

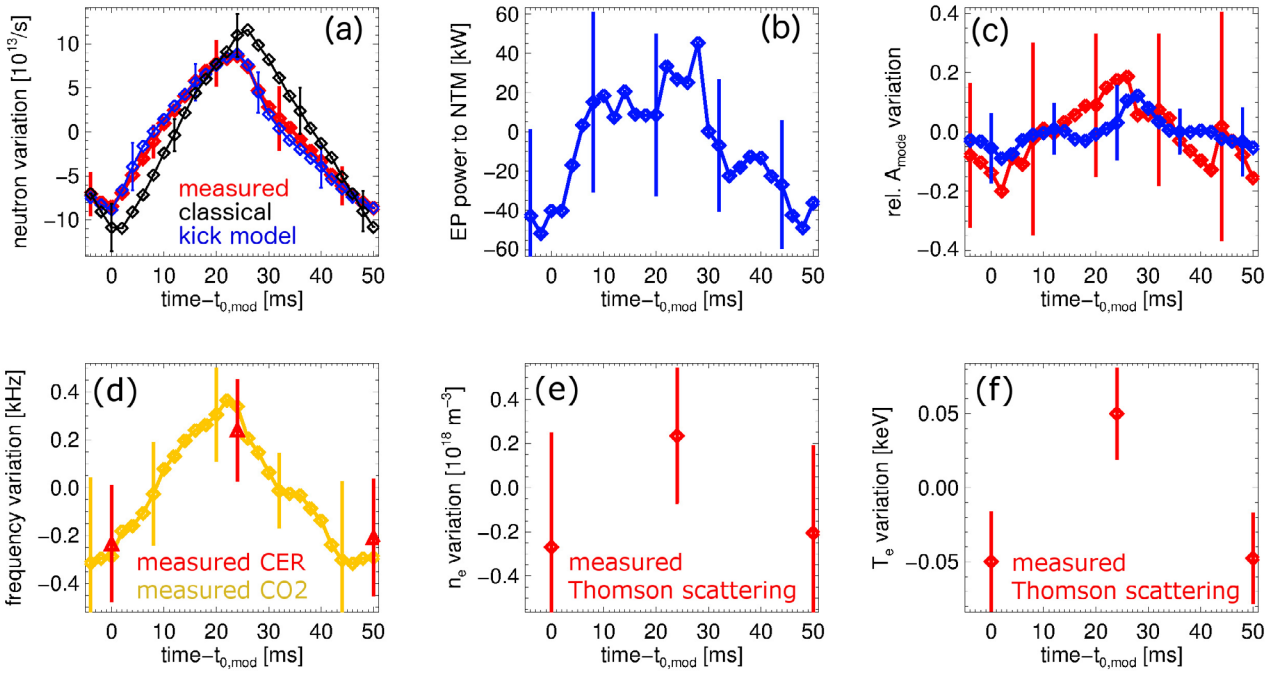

Figure 6. Results from conditional average analysis of DIII-D discharge #170247 for the time window $t = 3$–4 s. A single NB source is modulated with a square waveform with period of 50 ms and duty cycle 50%. The abscissa refers to the time delay with respect to the turn-on time of the modulated NB source. (*a*) Variation in neutron rate from measurements (red) and from TRANSP modeling (black, blue). The same color code applies to panels (*b*)–(*c*). (*b*) Variation of NB power flowing from NB ions to the NTM according to the kick model. (*c*) Relative change in mode amplitude. The experimental curve is computed from a CO2 interferometer signal. (*d*) Toroidal rotation frequency variation at the mode location from charge-exchange recombination (CER) spectroscopy and NTM frequency variation from CO2 interferometer data. (*e*) and (*f*) Variation of electron density and temperature near the mode location as measured through Thomson scattering.

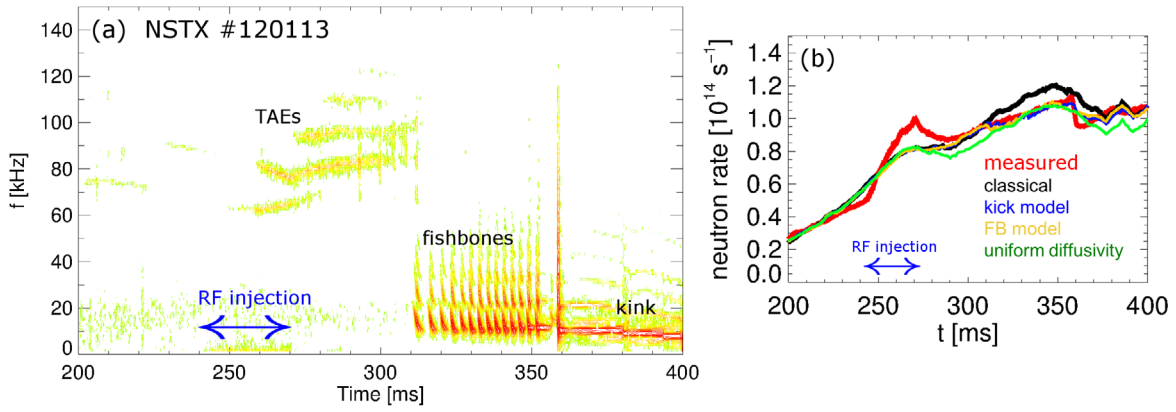

Figure 7. (*a*) Magnetic fluctuation spectrum for NSTX #120113. The time of interest is $t = 310$–360 ms, when only fishbones are observed. (*b*) Neutron rate from measurements (red) and from TRANSP simulations using the available models to introduce enhanced EP transport by fishbones.

3.2. Single-mode scenario: NSTX plasmas with unstable fishbones

Single-mode analysis has also been applied to NSTX discharges with unstable fishbones. The following example is based on the NSTX L-mode discharge #120113, see figure 7. A short phase of RF injection destabilizes TAE modes, which disappear during the time window of interest ($300 \leqslant t \leqslant 360$ ms) during which only fishbones are observed.

By tuning the simulation parameters, all three EP transport models (fishbone model in TRANSP, uniform diffusivity and kick model) can recover the measured neutron rate (figure 7(*b*). A fraction of 25% of particles affected by the instability or a diffusivity $D_b = 0.5$–1 m^2 s^{-1} give a reasonable agreement in terms of measured versus simulated neutron rate. For the kick model, mode amplitudes $\delta B_r/B \sim 1$–5 $\times 10^{-3}$ give reasonable match with the measured neutron rate, where δB_r is the perturbed radial magnetic field.

Although all three models can recover (by design) the measured neutron rate decrease, the inferred NB ion density and NB driven current profiles typically differ (figure 8). Profiles from the ad hoc diffusivity simulation simply resemble those from the classical run rescaled by 70%–80%.

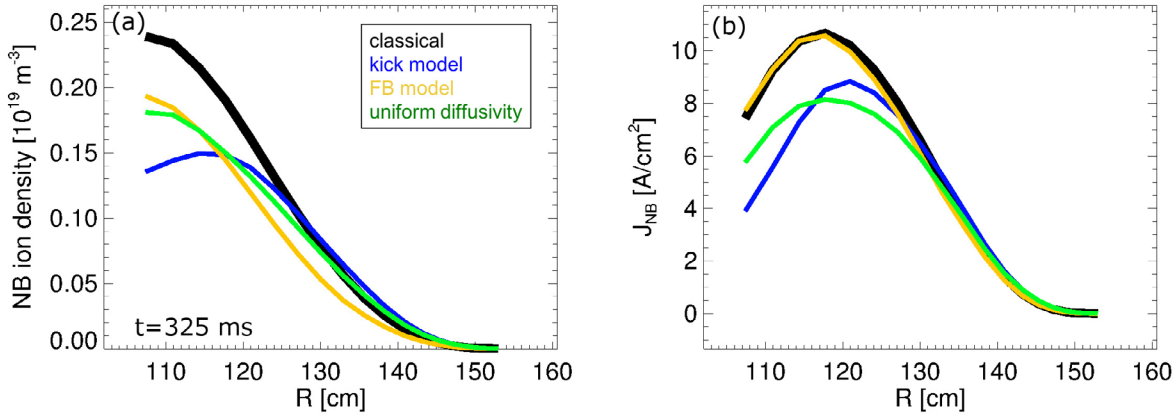

Figure 8. Radial profiles of (*a*) NB ion density and (*b*) NB-driven current density for NSTX #120113.

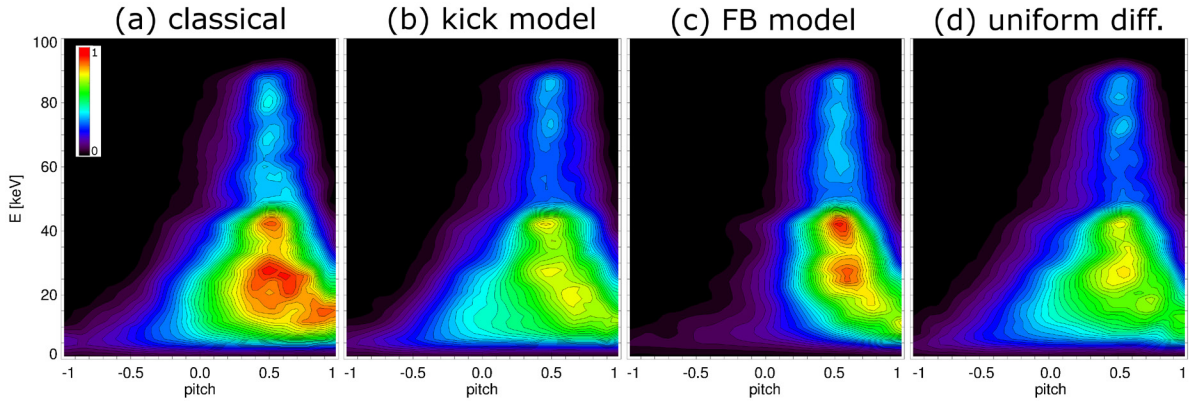

Figure 9. Fast ion distribution functions from NUBEAM/TRANSP for NSTX #120113 when different EP transport models are applied. Data from $t = 325$ ms are averaged over $120 \leqslant R \leqslant 130$ cm. All distributions are normalized by the same factor.

Because of their selectivity in phase space, the fishbone and kick model show more variability. However, density and NB driven current profiles are very different. For example, since the fishbone model only redistributes deeply trapped particles that contribute very little to the toroidal current, its NB driven current profile almost overlaps with that from the classical run. In contrast, the kick model is also redistributing co-passing particles, which results in a decrease of the core NB driven current.

Differences in integrals of the fast ion distribution, such as NB ion density and NB driven current density, can be understood by examining the fast ion distribution itself resulting from the different simulations (figure 9). Focusing around mid-radius, $120 \leqslant R \leqslant 130$ cm, the kick model computes a depletion of co-passing particles starting from the injection energy with respect to classical simulations. The uniform diffusivity run shows similar features. Conversely, the fishbone model computes a strong reduction in trapped particles (near pitch =0 in figure 9), while co-passing fast ions are nearly unaffected. These differences map directly on the resulting profiles, e.g. explaining the lack of degradation in NB driven current from the fishbone model since current is mostly driven by co-passing particles at large pitch.

More details on how the kick model affects the TRANSP simulation for fishbones are given in figure 10. For the NB injection parameters used in this discharge, NB deposition peaks near the axis with pitch ≈0.5–0.7. Most NB ions are co-passing, although some become trapped due to scattering and slowing down (figure 10(*a*)). Figures 10(*b*) and (*c*) show the root-mean-square energy kicks as a function of phase space variable resulting from ORBIT modeling for the fishbone mode. A large fraction of the fast ion phase populated by NB injection is characterized by finite interaction with the instability. In particular, ORBIT/kick model results show that both trapped and co-passing particles can drive the mode, in agreement with previous studies [46]. Hence, most particles experience enhanced transport, which explains the similar results obtained from the kick model and from the uniform diffusivity simulations (figures 9(*b*) and (*d*).

The analysis of scenarios with NTMs or fishbones is simplified by the reduced number of instabilities that have to be simulated. In contrast, scenarios with unstable AEs typically have to include a much larger number of modes, from 3–4 up to ∼20 or more. This translates to a very large number of (possibly overlapping) resonances with various strength that populate the fast ion phase space. Examples of TRANSP/kick model analysis of a DIII-D scenario with unstable AEs can be found in [38, 39]. Interpretive analysis with the kick model achieved a good match with the measured neutron rate [22] and a detailed comparison with FIDA signals was also performed [38]. TRANSP computes a slightly hollow fast ion density profile and a corresponding hollow FIDA brightness

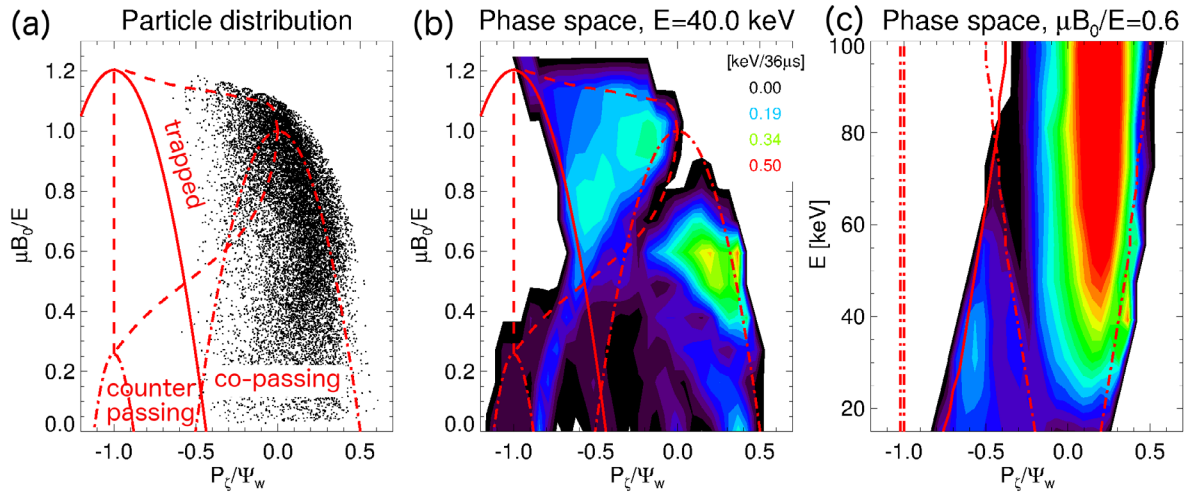

Figure 10. (*a*) Sample of the classical fast ion distribution for $E \geqslant 10$ keV at the beginning of the fishbone phase for NSTX #120113. Phase space boundaries are computed for $E = 40$ keV. (*b*)–(*c*) Examples of average energy kicks versus phase space coordinates for a $f = 14$ kHz fishbone mode in NSTX discharge #120113. Shown are two phase space cuts at (*b*) constant energy $E = 40$ keV and (*c*) constant $\mu B_0/E$ (normalized magnetic moment).

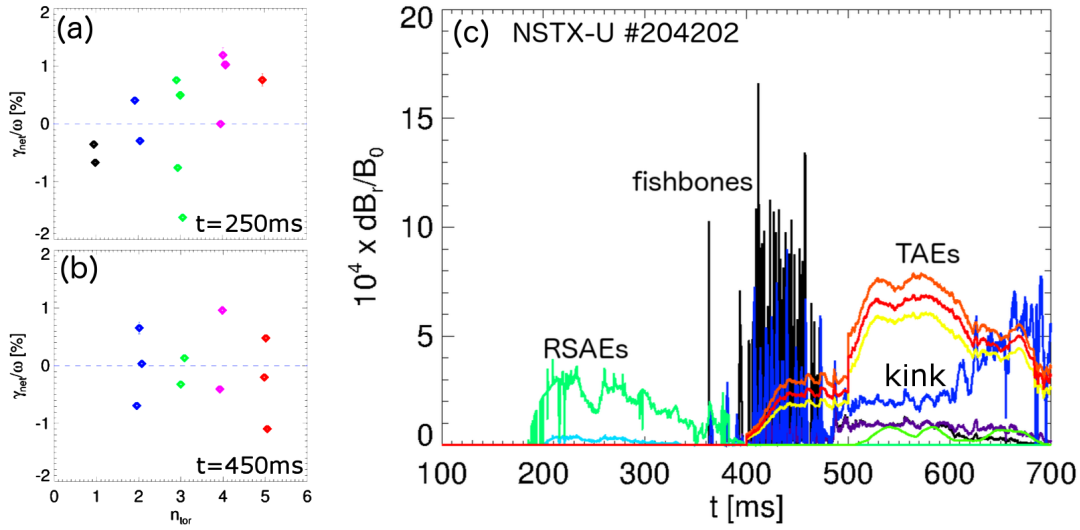

Figure 11. Estimate of mode stability and saturated amplitude for NSTX-U discharge #204202. (*a*)–(*b*) Net growth rate for AE modes around $t = 250$ ms and $t = 450$ ms. Colors indicate different toroidal mode numbers. (*c*) Peak $\delta B_r/B$ results for mode amplitude at saturation.

profile as a function of radius. Simulated FIDA features are in good quantitative agreement with the measurements. Given the complexity of the AE transport matrices once all resonances are included, it can be concluded that kick model is capturing the relevant wave-particle interaction and transport physics.

3.3. Multi-mode scenarios

The successful use of the reduced EP transport models for cases with a single type of instabilities is promising. A more challenging task is the analysis of scenarios with multiple types of instabilities simultaneously affecting fast ions. So far, this capability has been tested only for the kick model. (RBQ-1D relies on the theory of quasi-linear EP transport specifically developed for Alfvénic instabilities). Figure 1 shows an example of a NSTX-U discharge with coexisting AEs, fishbones and kink modes. The transport probabilities for each type of mode are computed through ORBIT. For AEs, radial mode structure is inferred from NOVA-K analysis at two representative times ($t = 250$ ms and $t = 450$ ms). Simple analytical expressions are used for kink and fishbones, as explained in section 3.2.

Even for interpretive analyses, the challenge for the TRANSP/kick model simulation is to consistently adjust the mode amplitudes, possibly as a function of time, since no direct mode amplitude measurements are available for this case. The procedure adopted in this work already hints at a possible use of the kick model (and, similarly, of RBQ-1D [22]) for predictive analysis. For AEs, NOVA-K provides the damping rate in addition to the radial mode structures. Dominant contributions to the damping rate are ion/electron Landau damping

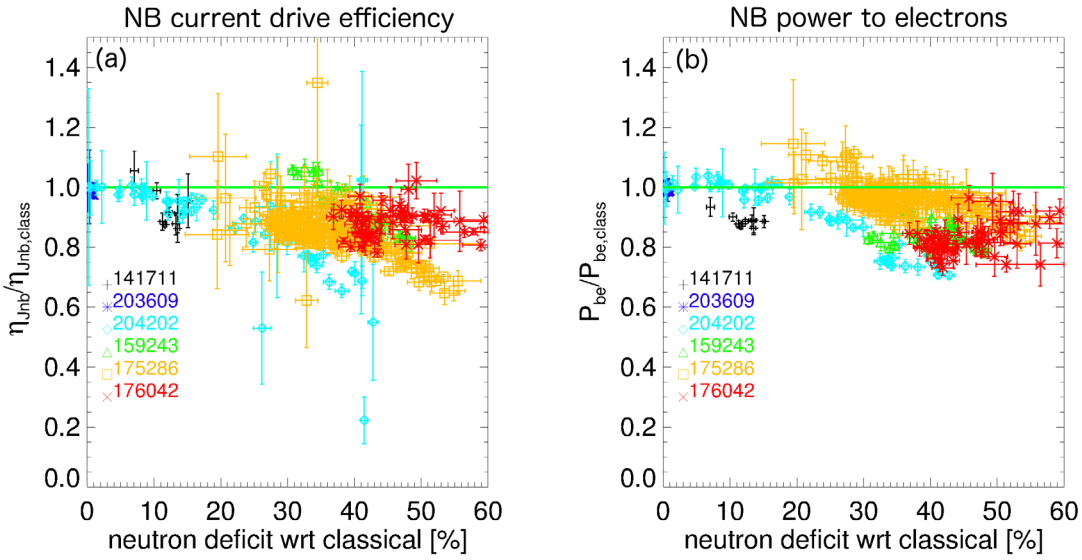

Figure 12. Comparison of (*a*) NB current drive efficiency and (*b*) NB power flowing to thermal electrons from a database of six NSTX, NSTX-U and DIII-D discharges featuring AE activity. The neutron rate deficit with respect to classical simulations on the abscissa is used as proxy for the overall severity of mode activity. Each point and its error bars represent average and standard deviation from a 10 ms time window. The NB current drive efficiency is here defined as $\eta_{Jnb} = I_{NB}/P_{NB}$ (ratio of total NB driven current over injected power). Shots #141711, 203609, 204202 are from NSTX/NSTX-U. Shots #159243, 175286, 176042 are from DIII-D.

and continuum damping. For TAE modes, radiative damping is also included. Since the power exchanged between fast ions and the $k-$ th mode, $P_{EP,k}$, can be calculated from the kick model [13], it is assumed that the saturated mode amplitude is such that $P_{EP,k}$ equals the power dissipated through damping, $P_{damp,k}$.

The linear AE growth rates inferred from the kick model for the case in figure 1(*a*) are shown in figures 11(*a*) and (*b*) for all candidate eigenmodes from NOVA-K with $n = 1$–6. Modes with positive (linear) growth rates are retained for the following analysis, in which AE mode amplitudes are gradually increased in a sequence of TRANSP runs and adjusted in time until the condition $P_{EP,k} = P_{damp,k}$ is verified at all times. This provides the expected AE saturation amplitude, see figure 11(*c*). Once AE amplitudes are known, fishbone and kink modes are added to the simulation. At present, damping rate is not available for these types of modes, therefore their amplitude is simply rescaled until good agreement with the measured neutron rate is achieved. TRANSP results for the neutron rate are shown in figure 1(*c*). As a comparison, the neutron rate obtained using a radially uniform, time dependent ad-hoc diffusivity for fast ions is also shown. Figure 1(*d*) illustrates the resulting fast ion density at the end of the fishbone sequence, $t \approx 450$ ms. As in the case discussed in section 3.2, the ad-hoc diffusivity results in a uniform decrease of the profiles with respect to classical simulations. The kick model predicts a larger effect of the instabilities in the core region, where fishbone amplitude is largest, and only negligible effects outside mid-radius.

Results from reduced EP transport models integrated in larger codes for integrated simulations, such as TRANSP, offer several advantages with respect to analyses performed on a single time-slice. As discussed in section 3.1, analysis of the dynamical response of fast ions to variations of the injected NB power [45] provides a powerful tool for both validation of EP transport models and assessment of fast ion transport and mode stability. Another advantage is a more complete picture of the discharge evolution, including a self-consistent treatment of the thermal plasma species and of the coupling between thermal and fast particles [1]. Focusing on discharges with unstable AEs only, figure 12 shows two examples of quantities that depend directly on the fast ion dynamic, but also affect the whole discharge evolution. In both cases, the neutron rate deficit with respect to classical simulations is used as a proxy for the severity of Alfvénic instabilities. The degradation in NB current drive efficiency with increasing AE activity is shown in figure 12(*a*). For the discharges included in the figure, the reduction in efficiency can be as large as 40%, which can lead to a substantial reduction in total plasma current for discharges with a large non-inductive current fraction. The second example (figure 12(*b*) shows the reduction in the power deposited from NB ions to thermal electrons through slowing-down. This term is critical in the overall power balance, as well as for the interpretation of local electron thermal transport coefficients, see additional example in figure 13.

4. Outlook of predictive use of the reduced models

The examples discussed in sections 3.1 and 3.2 are mostly limited to the interpretive use of the kick model. A central issue in the development of *predictive* capabilities is to infer the stability properties and resulting saturated amplitudes of the instabilities. A first example has been discussed in section 3.3 for NSTX-U discharge #204202, see figure 11. A second example is shown in figure 13 for an ensemble of discharges featuring unstable AEs from NSTX, NSTX-U and DIII-D. Results for the simulated neutron rate from predictive kick model analysis compared to measurements are

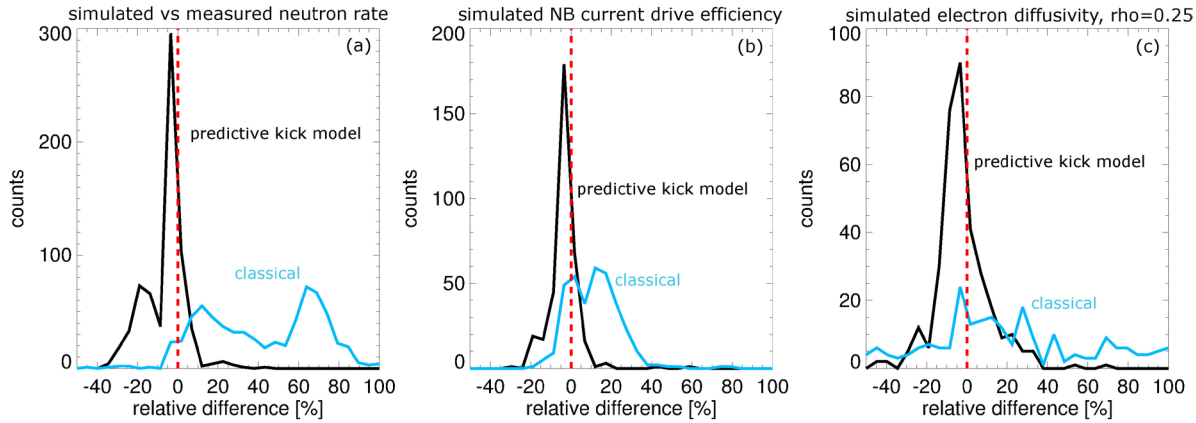

Figure 13. (*a*) Relative difference between measured and simulated neutron rate using predictive kick model analysis (black) and classical runs (cyan). (*b*)–(*c*) Relative difference with respect to interpretive analysis results from predictive (black) and classical (cyan) simulations for NB current drive efficiency, η_{Jnb}, and electron thermal diffusivity at normalized radius $\rho = 0.25$.

summarized in figure 13(*a*), showing that the analysis can recover the measured neutron rate typically well within $\pm$ 10%. Overall, predictive results are also in good agreement with those from interpretive simulations. In this case, the comparison is performed for derived quantities, such as NB current drive efficiency and inferred electron thermal diffusivity, for which no direct measurement is available. Therefore, the comparison takes results from the interpretive analysis as reference. Figures 13(*b*) and (*c*) show the difference in NB current drive efficiency and local electron thermal diffusivity between interpretive and predictive simulations. The (larger) difference between interpretive and classical simulations is also shown for comparison.

A challenge in the predictive simulations is the calculation of stability and saturation levels over time scales of the order of—or longer than—typical fast ion slowing down times (from 10's of milliseconds to seconds). To this end, the analysis should take into account self-consistently possible variations of the background plasma profile, for example density and temperature (also affecting the damping rate) or q-profile (affecting the radial mode structure). Simulations that recompute the mode properties as time evolves are still computationally very expensive [47–50]. A reduced approach for codes such as TRANSP is presently under consideration. In spite of these difficulties, reduced models already represent an effective alternative to first-principles codes for scenario development, when accuracy in the prediction of EP-driven instabilities and associated transport is sacrificed in favor of the integration of those effects into the bigger picture of *integrated modeling* [1].

5. Conclusions

The inclusion of reduced EP transport models in TRANSP is resulting in improved interpretive and predictive capabilities for long time scale time-dependent integrated tokamak simulations. Including the effects of EP transport by instabilities is crucial for the accurate, quantitative computation of the heat and momentum sources, which also affect thermal transport calculations and predictions. This work extends previous studies focusing on Alfvénic modes to lower-frequency instabilities such as NTMs and fishbones. An important result is that those different types of instabilities can show synergistic effects through their modifications of the fast ion distribution function. Accurate time-dependent simulations need to include all types of instabilities consistently within the same simulation.

Over the last few years, the kick model has been successfully applied to analyze EP transport on NSTX/NSTX-U and DIII-D. Its integration with the TRANSP code has made continuous progress, along with the development of diagnostics tools in TRANSP to facilitate the comparison between code predictions and experimental data. Work is also ongoing to complement the kick model approach with the RBQ-1D model based on recent improvements to the original quasi-linear theory [14, 22]. RBQ-1D is based on the resonance-broadening quasi-linear theory and can address the need for a self-consistent, predictive transport model for integrated simulations. Initial benchmark between kick and RBQ-1D models shows good agreement in terms of predicted EP transport. As discussed in this work, recent efforts are extending the kick model capabilities to account for MHD instabilities other than Alfvénic modes, such as NTMs, kinks, fishbones and sawteeth. Interpretive analysis is already possible. Predictive analysis will require additional modeling to estimate the damping rate of those instabilities, as already done for AE modes through NOVA/NOVA-K. Validation across multiple devices is ongoing and will be reported in future publications. In general, enhancements to TRANSP by including reduced EP transport models have already enabled scenario development and predictions that include a realistic treatment of fast ion transport by instabilities.

Acknowledgments

The NSTX-U and DIII-D Teams are gratefully acknowledged for their support in all experimental aspects of the research presented in this work. This manuscript has been authored by Princeton University and is based upon work supported by the U.S. Department of Energy, Office of Science, Office of

Fusion Energy Sciences, under Contract Numbers DE-AC02-09CH11466 and DE-FC02-04ER54698 with the U.S. Department of Energy. Neither the United States Government nor any agency thereof, nor any of their employees, makes any warranty, express or implied, or assumes any legal liability or responsibility for the accuracy, completeness, or usefulness of any information, apparatus, product, or process disclosed, or represents that its use would not infringe privately owned rights. Reference herein to any specific commercial product, process, or service by trade name, trademark, manufacturer, or otherwise, does not necessarily constitute or imply its endorsement, recommendation, or favoring by the United States Government or any agency thereof. The views and opinions of authors expressed herein do not necessarily state or reflect those of the United States Government or any agency thereof.

DIII-D data shown in this paper can be obtained in digital format by following the links at https://fusion.gat.com/global/D3D_DMP. NSTX/NSTX-U data can be found following the links from http://arks.princeton.edu/ark:/88435/dsp018p58pg29j.

ORCID iDs

M. Podestà https://orcid.org/0000-0003-4975-0585
W.W. Heidbrink https://orcid.org/0000-0002-6942-8043
V.N. Duarte https://orcid.org/0000-0001-8096-7518
G.J. Kramer https://orcid.org/0000-0001-5105-8139
D. Kim https://orcid.org/0000-0002-6085-9525
D. Liu https://orcid.org/0000-0001-9174-7078
F.M. Poli https://orcid.org/0000-0003-3959-4371
M.A. Van Zeeland https://orcid.org/0000-0002-7911-2739

References

[1] Poli F.M. 2018 *Phys. Plasmas* **25** 055602
[2] Fasoli A. *et al* 2007 Progress in the ITER Physics Basis Chapter 5: Physics of energetic ions *Nucl. Fusion* **47** S264
[3] Heidbrink W.W. 2008 *Phys. Plasmas* **15** 055501
[4] Sharapov S. *et al* 2013 *Nucl. Fusion* **53** 104022
[5] Gorelenkov N. *et al* 2014 *Nucl. Fusion* **54** 125001
[6] McClements K.G. *et al* 2017 *Plasma Phys. Control. Fusion* **59** 053001
[7] Menard J.E. *et al* 2012 *Nucl. Fusion* **52** 083015
[8] Chen L. *et al* 2016 *Rev. Mod. Phys.* **88** 015008
[9] Ghantous K. *et al* 2012 *Phys. Plasmas* **19** 092511
[10] Waltz R.E. *et al* 2015 *Nucl. Fusion* **55** 123012
[11] Gorelenkov N.N. *et al* 2016 *Nucl. Fusion* **56** 112015
[12] Duarte V.N. *et al* 2017 *Nucl. Fusion* **57** 054001
[13] Podestà M. *et al* 2017 *Plasma Phys. Control. Fusion* **59** 095008
[14] Gorelenkov N.N. *et al* 2018 *Nucl. Fusion* **58** 082016
[15] Breslau J. *et al* 2018 TRANSP (Computer Software) (https://doi.org/10.11578/dc.20180627.4)
[16] Hawryluk R.J. 1980 *Physics of Plasmas Close to Thermonuclear Conditions* (Brussels: CEC)
[17] Goldston R.J. *et al* 1981 *J. Comput. Phys.* **43** 61
[18] Pankin A. *et al* 2004 *Comput. Phys. Commun.* **159** 157
[19] Podestà M. *et al* 2014 *Plasma Phys. Control. Fusion* **56** 055003
[20] Berk H.L. *et al* 1996 *Phys. Plasmas* **3** 1827
[21] Berk H.L. *et al* 1995 *Nucl. Fusion* **35** 1661
[22] Gorelenkov N.N. *et al* 2019 *Phys. Plasmas* **26** 072507
[23] Vedenov A.A. *et al* 1961 *Sov. Phys.—Usp.* **4** 332
[24] Drummond W.E. *et al* 1962 *Nucl. Fusion Suppl.* **3** 1049
[25] Luxon J.L. 1985 *Fusion Sci. Technol.* **48** 828
[26] Heidbrink W.W. *et al* 2018 *Nucl. Fusion* **58** 082027
[27] BardÓczi L. *et al* 2019 *Plasma Phys. Control. Fusion* **61** 055012
[28] Kim D. *et al* 2018 *Nucl. Fusion* **58** 082029
[29] White R.B. 2006 *The Theory of Toroidally Confined Plasmas* 2nd edn (London: Imperial College Press)
[30] White R.B. 2012 *Commun. Nonlinear Sci. Numer. Simulat.* **17** 2200
[31] White R.B. *et al* 1984 *Phys. Fluids* **27** 2455
[32] Cheng C.Z. 1992 *Phys. Rep.* **1** 211
[33] Fu G.Y. *et al* 1992 *Phys. Fluids* B **4** 3722
[34] Gorelenkov N.N. *et al* 1999 *Phys. Plasmas* **6** 2802
[35] White R.B. 2013 *Phys. Plasmas* **20** 022105
[36] Carolipio E.M. *et al* 2002 *Nucl. Fusion* **42** 853
[37] Glasser A.H. *et al* 2016 *Phys. Plasmas* **23** 112506
[38] Heidbrink W.W. *et al* 2017 *Phys. Plasmas* **24** 056109
[39] Collins C.S. *et al* 2016 *Phys. Rev. Lett.* **116** 095001
[40] Podestà M. *et al* 2018 *Nucl. Fusion* **58** 082023
[41] BardÓczi L. *et al* 2017 *Phys. Plasmas* **24** 122503
[42] BardÓczi L. *et al* 2016 *Phys. Plasmas* **23** 052507
[43] Muscatello C.M. *et al* 2010 *Rev. Sci. Instrum.* **81** 10D316
[44] Heidbrink W.W. *et al* 2006 *Rev. Sci. Instr.* **77** 10F120
[45] Heidbrink W.W. *et al* 2016 *Nucl. Fusion* **56** 112011
[46] Fredrickson E.D. *et al* 2003 *Nucl. Fusion* **43** 1258
[47] Park W. *et al* 1999 *Phys. Plasmas* **6** 1796
[48] Lang J. *et al* 2009 *Phys. Plasmas* **16** 102101
[49] Todo Y. *et al* 2012 *Nucl. Fusion* **52** 094018
[50] Todo Y. *et al* 2016 *Nucl. Fusion* **56** 112008